Detailed low-energy electron diffraction analysis of the (4 × 4) surface structure of C_{60} on Cu(111): Seven-atom-vacancy reconstruction

Geng Xu,[1,2] Xing-Qiang Shi,[1,*] R. Q. Zhang,[1] Woei Wu Pai,[3,†] H. T. Jeng,[4,5] and M. A. Van Hove[1,*,†]

[1]*Department of Physics and Materials Science, City University of Hong Kong, Kowloon, Hong Kong, China*

[2]*Physics Department, Zhongshan (Sun Yat-Sen) University, Guangzhou, China*

[3]*Center for Condensed Matter Science, National Taiwan University, Taipei 106, Taiwan*

[4]*Institute of Physics, Academia Sinica, Taipei, Taiwan*

[5]*Department of Physics, National Tsing Hua University, Hsinchu 300, Taiwan*

(Received 9 July 2012; published 8 August 2012; publisher error corrected 15 August 2012)

A detailed and exhaustive structural analysis by low-energy electron diffraction (LEED) is reported for the C_{60}-induced reconstruction of Cu(111), in the system Cu(111) + (4 × 4)-C_{60}. A wide LEED energy range allows enhanced sensitivity to the crucial C_{60}-metal interface that is buried below the 7-Å-thick molecular layer. The analysis clearly favors a seven-Cu-atom vacancy model (with Pendry R-factor $R_p = 0.376$) over a one-Cu-atom vacancy model ($R_p = 0.608$) and over nonreconstructed models ($R_p = 0.671$ for atop site and $R_p = 0.536$ for hcp site). The seven-Cu-atom vacancy forms a (4 × 4) lattice of bowl-like holes. In each hole, a C_{60} molecule can nestle by forming strong bonds (shorter than 2.30 Å) between 15 C atoms of the molecule and 12 Cu atoms of the outermost and second Cu layers.

DOI: 10.1103/PhysRevB.86.075419 PACS number(s): 61.05.jh, 68.35.bp, 68.35.Ct, 68.43.−h

I. INTRODUCTION

Fullerene-based molecular crystals on metals are of interest because of their unique electronic properties, which are influenced by the atomic structure of the interface between the molecules and the metal. C_{60} adsorption has been studied on several metal surfaces,[1] including Ag(111),[2] Al(111),[3] and Pt(111):[4,5] these metals were found to reconstruct into a one-metal-atom vacancy structure, in which one metal atom is missing under each C_{60} molecule. A study of C_{60} on Cu(111) performed by Pai *et al.*[6] found that after deposition of C_{60} and annealing to 500 K, the C_{60} molecules sink into the Cu(111) surface by ∼2 Å, which is close to the Cu(111) interlayer spacing. This suggested that Cu atoms are missing to form a sufficiently wide one-layer-deep hole under every C_{60} molecule. A subsequent mass-flow analysis by *in situ* scanning tunneling microscope (STM) monitoring of C_{60} growth[7] suggested that, in each (4 × 4) unit cell, seven Cu atoms were removed from the outermost Cu layer, enough to form such a hole.

An important further study by Pai *et al.*[8] used first-principles density functional theory (DFT) calculations to evaluate the electronic structure of this system with the seven-Cu-atom-vacancy model, and used low-energy electron diffraction (LEED) to perform an initial structural search. The results indicated a charge transfer of about $3e^-$ per C_{60} molecule, in excellent agreement with experiments of photoelectron spectroscopy (PES) and scanning tunneling spectroscopy (STS).[8] In that work, the geometry of the interface structure obtained by total energy calculation was supported by our initial LEED analysis based on a limited experimental database.

However, that earlier LEED analysis can be considerably improved. In particular, since the molecule/metal interface is located about 7 Å below the tops of the C_{60} molecules, i.e. at a depth comparable to the electron mean-free path, it is helpful to increase the sensitivity of the interface analysis by using higher-energy incident electrons that can penetrate deeper below the molecules. The higher energies also provide a larger database of experimental LEED intensities, to which the many structural parameters of this system (about 100) can be fit with greater accuracy.

In Sec. II, we present our LEED experiment at 185 K with 40–400 eV incident electron energies. In Sec. III, the LEED analysis methodology is described. Section IV presents the resulting geometric results, which are discussed in Sec. V. Conclusions are in Sec. VI.

II. EXPERIMENT

The Cu(111) + (4 × 4)-C_{60} structure is readily prepared. The Cu(111) surface was cleaned by repeated cycles of sputtering and annealing (at 600 °C). The cleaned surface showed wide terraces, typically >100 nm, in STM images. C_{60} was evaporated from a homemade tantalum crucible, with a slow deposition rate ∼0.05 to 0.1 monolayer (ML) per min and a low background pressure below 1×10^{-10} torr. During dosing, the sample was held at ∼500 K. A slight excess C_{60} coverage (>1 ML) was dosed, followed by annealing at ∼600 K, to obtain a well-ordered (4 × 4) structure without multilayers. Scanning tunneling microscope images revealed two C_{60} orientation domains, as discussed in Ref. 6. The typical domain size is on the order of 100 nm.

Samples prepared with the above procedure showed a sharp LEED pattern, illustrated in Fig. 1. To obtain LEED I-V data, we used a commercial Omicron SpectaLEED and a commercial CMOS camera. To improve our previous room-temperature LEED I-V analysis reported in Ref. 8, we cooled the sample down to 185 K and extended the LEED energy range from 45 to 400 eV. The LEED pattern was photographed for every 0.5 eV beam energy change under normal incidence condition. We developed a code to automatically track the same beam spot across consecutive LEED photos. The beam intensity was calculated from the integration of a background-subtracted 2D fitted Gaussian beam profile. The raw LEED

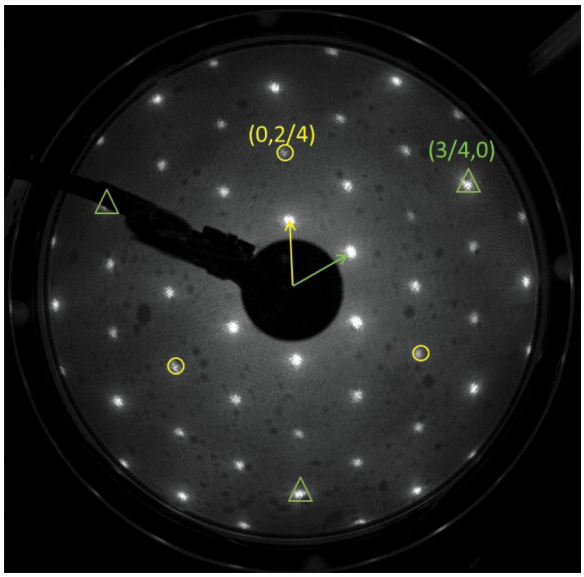

FIG. 1. (Color online) LEED pattern of Cu(111) + (4 × 4)-C_{60} (beam energy = 45 eV, normal incidence). The pattern has C_{3v} symmetry. The two arrows point at beams (1/4,0) and (0,1/4). Two sets of fractional-order spots, which are symmetry-equivalent at normal incidence, are denoted by triangles and circles, respectively, with some beam indices labeled. Integer-order spots are off the screen.

intensity data were then corrected for the LEED screen transmittance, the camera's optical response to beam intensity, and the beam current. The LEED pattern shows the expected C_{3v} symmetry, reflecting the domain averaging and substrate symmetry. Consequently, all equivalent LEED beams were averaged. We note that the I-V curves of all equivalent beams are quite similar, indicating good data quality. The averaged I-V curves are listed in supplementary material I.[9]

III. LEED ANALYSIS

The earlier DFT calculations[10] clearly suggest that the C_{60} buckyballs favor bonding to the Cu(111) surface through a hexagonal face (as opposed to a pentagonal face that would match the substrate symmetry less well). The STM images also suggest this,[6] because the images of the C_{60} molecule reveal threefold symmetry. The DFT calculations also indicate that the adsorption symmetry of C_{60} on Cu(111) reduces the clean-metal symmetry from C_{3v} to C_3,[8,10] suggesting that threefold rotational symmetry is retained while the mirror symmetries of the substrate and molecule are broken. Even though C_{60} also has C_{3v} symmetry around axes perpendicular to its hexagonal faces, the DFT calculations imply that its mirror planes do not coincide with those of the Cu(111) substrate; consequently, two structurally equivalent mirrored domain orientations must be formed on the Cu(111) surface, as observed in the STM experiment.[6] The LEED pattern nevertheless exhibits mirror plane symmetry, obtained by averaging over the two domain orientations, each domain having C_3 symmetry. The LEED fit assumed this C_3 symmetry and equal domain orientations.

The symmetrized automated tensor LEED computer code SATLEED[11–13] was used for the structure analysis. This allows fitting relatively many adjustable parameters using an efficient automated search procedure. We describe next the geometrical treatment of the seven-atom-vacancy model of Cu(111) + (4 × 4)-C_{60} with this code; other structural models are treated similarly.

For LEED computational purposes, the seven-atom-vacancy model is decomposed into five layers totaling 101 adjustable atoms per (4 × 4) unit cell. The C_{60} molecules can be sliced parallel to the surface into three composite layers having 21, 18, and 21 carbon atoms per molecule in the outermost, middle, and inner layers, respectively. Since the C_{60} molecule sinks into the seven-atom hole of the first Cu layer, its innermost layer of six C atoms is nearly coplanar with the outermost Cu layer, which has (4 × 4) − 7 = 9 atoms per (4 × 4) unit cell. We therefore combine the 21 inner C atoms and these nine Cu atoms into a single mixed composite layer of 30 atoms per cell. The second Cu layer has 16 Cu atoms per (4 × 4) unit cell, and so does the third Cu layer. All atomic coordinates in these five composite layers (with 21 + 18 + 30 + 16 + 16 = 101 atoms in total) were adjusted by automated search, assuming threefold rotational symmetry, without imposing mirror symmetry. The assumed C_3 symmetry results in 101 adjustable coordinates and one nonstructural parameter (the inner potential), totaling 102 independent adjustable parameters in this model (not counting discrete variations of layer-dependent Debye temperatures, perpendicular vs parallel vibrational amplitudes and imaginary parts of the inner potential described below).

Due to the relatively low total electron density of C_{60} compared to the metal substrate, one must expect a relatively longer electron mean-free path in the outer parts of the molecule. In the absence of corresponding measurements, we adopt a stepwise decreasing mean-free path from layer to layer, represented by an increasing imaginary part of inner potential with values −2.5, −2.5, and −3.5 eV, respectively, for the first three composite layers going inward, followed by −4.5 eV for deeper layers, including the Cu bulk. This variable damping required modifying the standard SATLEED code. Compared to using a homogeneous imaginary part of the inner potential of −4.5 eV in all layers, the resulting best-fit atomic coordinates changed by at most 0.02–0.03 Å, which is well within all error bars.

As is frequently done in LEED, first the structural parameters (and inner potential) are fit to the data, before also fitting thermal parameters in a more approximate manner, as the optimum structure depends less on these parameters: in the case of SATLEED, the Debye temperature (θ_D) and the atomic enhancement factors for the mean square vibrational amplitudes perpendicular and parallel to the surface (F_{per}, F_{par}) have been modified to improve the fitting by testing a few different values. Finally, we obtained θ_D = 1000 K for the C atoms, θ_D = 343 K for the Cu atoms, $F_{\mathrm{per}} = F_{\mathrm{par}} = 1.0$ for all Cu atoms, and some C atoms located at the interface and bonded to Cu atoms, while $F_{\mathrm{per}} = F_{\mathrm{par}} = 3.0$ is better for the C atoms which do not bond to Cu atoms, implying stronger vibrations that are approximately isotropic.

In our analysis, a maximum angular momentum l_{max} = 11 was used, so 23 partial waves were taken into account: this is appropriate for higher electron energies up to 400 eV. The phase shifts were obtained by the atomic overlapping approach, with a Cu crystal environment for all Cu atoms,

with a C monolayer on a simple Cu surface for the C atoms located at the interface, and with a bulk graphite environment for C atoms which do not bond to Cu.

We used 30 symmetrically inequivalent diffracted beams obtained by experiment, with a total (cumulative) energy range of 7111 eV, for comparison with the theoretical LEED I-V curves.

We used two different estimates of the accuracy of structure determination by LEED,[14] the first reflecting precision due to internal consistency of the data, while the second better reflects the accuracy of the methodology as a whole; this also ensures that our structural results are not significantly affected by the choice of estimates in the presence of a relatively large number of adjustable parameters. In the first method, applied to LEED by Shih *et al.*,[15] the n-independent LEED beams are considered to be independent experiments. Assume that the ith beam taken alone yields a best-fit value y_i of a certain parameter y (for example, a certain bond length), and that this beam is given a weight w_i proportional to its energy range ΔE_i. Then the overall square standard deviation S^2 for this parameter is:

$$S^2 = \frac{n\sum_{i=1}^{n} w_i (y_i - \bar{y})^2}{(n-1)}. \quad (1)$$

Here, $\bar{y} = \sum_{i=1}^{n} w_i y_i$ is the arithmetic mean of the values y_i and $w_i = \frac{\Delta E_i}{\sum_{i=1}^{n} \Delta E_i}$. Then, using the student's t-distribution,[16] the error bar Δy of parameter y is:

$$\Delta y = \pm \mathrm{S} \text{ with a } 68\% \text{ confidence level;}$$

$$\Delta y = \pm 2\mathrm{S} \text{ with a } 95\% \text{ confidence level.}$$

A more common estimate of accuracy in LEED structure determination follows Pendry's approach.[17] It views LEED I-V curves as composed of N experimental Lorentzian peaks to be fit with theory using an R-factor R (which measures the discrepancy between theory and experiment) that will vary about a mean value. The double reliability factor RR was defined by Pendry to indicate the reliability of reliability factors:

$$RR = \frac{\mathrm{var}\, R_N}{\bar{R}_N}. \quad (2)$$

Here, N is the number of well-separated experimental peaks in the total energy range ΔE, var R_N is the standard square deviation of the R-factor, and $\bar{R}_N$ is the overall mean R-factor. The value of N can be approximated as

$$N = (\Delta E/4\,|V_{0i}|), \quad (3)$$

where V_{oi} is the (average) imaginary part of the inner potential. We can apply Eqs. (2) and (3) to obtain the standard square deviation for a fit parameter d as:[12]

$$\mathrm{var}\,(d) = \frac{\varepsilon R_{\min}}{\sqrt{\frac{N}{8}}}. \quad (4)$$

Here, $1/\varepsilon$ is the curvature of $R(d)$ near the minimum $R_{\min}$ and is thus the second derivative of $R(d)$ at that minimum: $(1/\varepsilon) = R''_{\min}(d)$. Typically, the Pendry approach of Eq. (4) is relatively conservative and, in particular, gives error bars that are three to six times larger than those of Shih *et al.*, Eq. (1).

TABLE I. Structures tested by LEED for Cu(111) + (4 × 4)-C_{60}, with corresponding R-factors; r-fcc and r-hcp indicate reconstructions with missing metal atoms, r-hcp having the outermost Cu layer in a hcp stacking sequence relative to the underlying bulk.

Structure model	R-factor R_P
C_{60} molecule on-top site, nonreconstructed	0.671
C_{60} molecule on hcp site, nonreconstructed	0.536
One-Cu-atom vacancy of r-fcc	0.608
Seven-Cu-atom vacancy of r-fcc (Ref. 8) with Cu(BCABCA. . .) fcc stacking	0.376
Seven-Cu-atom vacancy of r-hcp (Ref. 8) with Cu(BCBACBA. . .) hcp stacking	0.455

We used the Pendry R-factor R_P for automated optimization of all structural coordinates.[17]

IV. GEOMETRICAL RESULTS

We tested several possible models for Cu(111) + (4 × 4)-C_{60}, listed in Table I. STM images imply that the buckyballs are oriented such that a C hexagon lies parallel to the substrate surface, with an azimuthal direction close to the crystallographic axes of the substrate. The DFT calculations also support this observation.

For each model in Fig. 2, the LEED analysis started with C_{60} positioned at a variety of heights above the metal surface, and then allowed full relaxations within the molecule and two outermost metal layers, assuming threefold rotational symmetry. The LEED-optimized relaxations were used in all our figures.

Figure 2(a) shows the best-fit result for the nonreconstructed on-top adsorption model, giving an unfavorable $R_p = 0.671$, with distances 2.01 and 2.32 Å between six pairs of C and Cu atoms, and with distances 1.91 and 2.01 Å from 6 C to the central Cu atom. While these bond lengths are reasonable, the large R_p value compared to that for the best-fit seven-Cu-atom vacancy model and the large distortions within the C_{60} molecule [cf. Fig. 2(a)] compared to the DFT results rule out this model. It should be noted that it is common for incorrect models to produce unrealistic distortions that are incompatible with total-energy calculations. The total energy calculations for this model strongly favor the particular

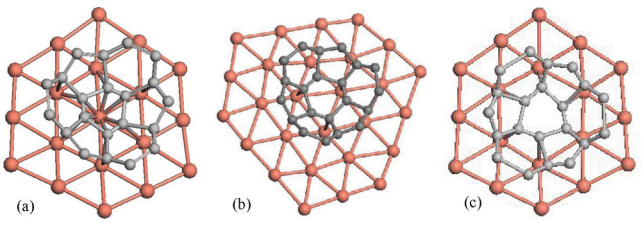

FIG. 2. (Color online) Three models for Cu(111) + (4 × 4)-C_{60}, viewed slightly off-normal, showing only atoms in the topmost Cu layer (large red balls) and the bottom 21 atoms of the buckyball (small gray balls), as optimized with LEED. (a) Nonreconstructed on-top adsorption (i.e. with the buckyball axis above a Cu surface atom): $R_p = 0.671$. (b) Nonreconstructed hcp-site adsorption (i.e. with the buckyball axis at an hcp hollow site): $R_p = 0.536$. (c) One-Cu-atom vacancy model: $R_p = 0.608$.

azimuthal orientation of C_{60} shown in Fig. 2(a),[10] so other orientations were not considered by LEED.

Figure 2(b) illustrates nonreconstructed hcp-site adsorption after optimization, giving $R_p = 0.536$, with distances of 2.31 Å between three pairs of C and Cu atoms. This large R-factor value also rules out this model.

Figure 2(c) shows an optimized reconstructed model with a one-Cu-atom vacancy below the center of each C_{60} molecule, similar to the structures reported for C_{60}/Ag(111), C_{60}/Al(111), and C_{60}/Pt(111).[2–5] The best-fit result gives $R_P = 0.608$, with distances 1.98 and 2.29 Å between six pairs of C and Cu atoms. Figure 2(c) shows that the distortion of the C_{60} molecule is severe, which is again not compatible with DFT calculations.

For the seven-atom-vacancy model of Cu(111) + (4 × 4)-C_{60}, we explored two basic alternatives: in one model, r-fcc, the Cu atoms kept their bulklike fcc arrangement, while in the other, r-hcp, the nine outermost Cu atoms per unit cell adopted hcp positions relative to the underlying Cu layers. In our DFT calculation,[8] the energy difference between these two models is remarkably small. The r-hcp model is preferred by ∼0.01 eV/cell if the Cu slab used in calculation is thinner than ∼15 Cu layers. For thicker slabs (from 18 to 30 Cu layers), the r-fcc structure becomes ∼0.02 eV/cell lower in energy. As we shall see, our LEED analysis can distinguish clearly between these models, despite the depth of the differing atoms, namely in the third and deeper metal layers.

For the r-fcc model, we used the Cu(BCABCA...) layer stacking in the LEED analysis, while the equivalent Cu(BACBAC...) stacking was used in the earlier DFT calculations,[8] corresponding simply to a rotation of the whole sample by 180°. For the r-hcp model, we assumed Cu(BCBACBA...) stacking in the LEED analysis. We used the optimum coordinates obtained by the DFT calculation[8] for the top three layers (60 C atoms and nine Cu atoms of the first B layer) as the starting point for the LEED fitting, while the deeper layers were initially given the bulk structure. A total of 102 independent parameters were relaxed automatically to optimize the Pendry R-factor. As is common with tensor LEED, this process was iterated several times until the search had converged.

The best-fit geometry gave a Pendry R-factor of 0.455 for r-hcp and 0.376 for r-fcc, thus strongly favoring r-fcc. For r-fcc, the best-fit inner potential is 5.11 eV; the optimized coordinates of the 101 adjusted atoms are listed in supplementary material II.[18] Figure 3 shows the best overall fit between theory and experiment for the 30 independent beams used. Figure 4 gives a top view of the LEED-optimized structure of Cu(111) + (4 × 4)-C_{60}, while Fig. 5 gives a near-grazing close-up view of the interface region between substrate and molecule.

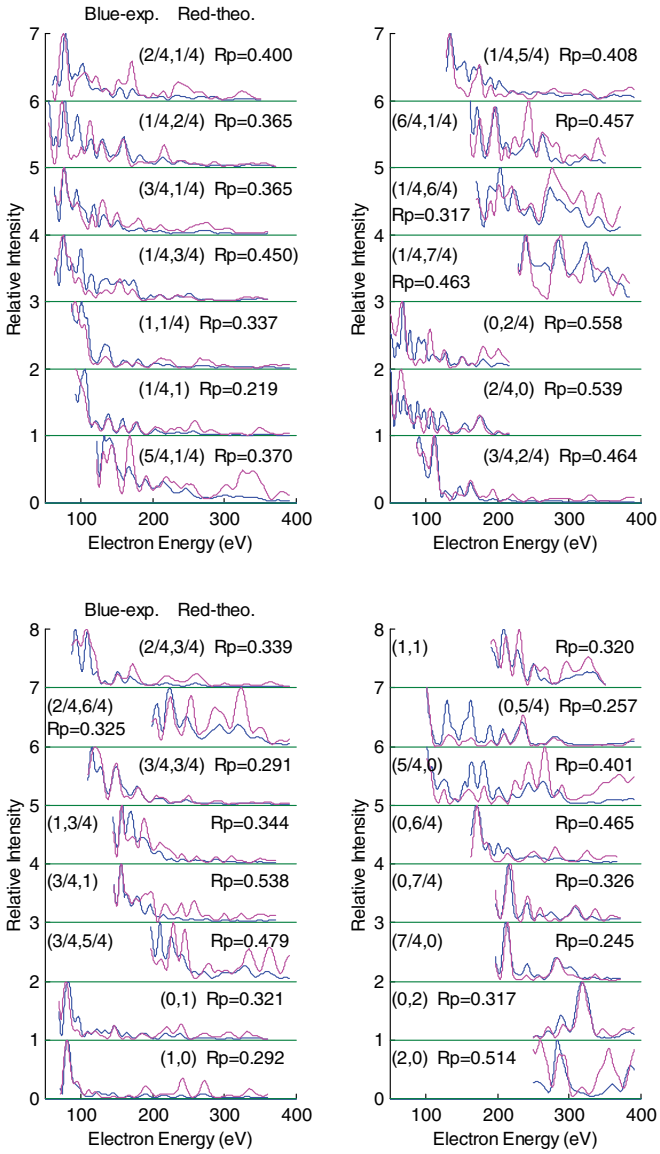

FIG. 3. (Color online) Theoretical (red/gray) and experimental (blue/medium gray) intensity-voltage curves for the 30 independent beams used in the LEED analysis for the best-fit r-fcc seven-atom-vacancy model of Cu(111) + (4 × 4)-C_{60}. Individual Pendry R-factors are shown for each beam; the overall beam-averaged Pendry R-factor is 0.376. The intensities have been normalized so each curve has a maximum intensity of 1.

V. DISCUSSION

Our new LEED results presented here strongly support the previous work with DFT[8] and further confirm and detail our earlier conclusions from LEED.

We first compare the atomic positions from DFT and LEED for the best-fit structure r-fcc shown in Figs. 4 and 5; the complete sets of optimized coordinates are listed in supplementary material II, Part 2.[18] The different coordinate systems used in the DFT and LEED calculations offered an opportunity to test the reproducibility of the LEED optimization process itself, by repeating the complete LEED optimization after rotation of the sample and beams by 180°: we obtained $R_p = 0.377$ vs 0.376 and differences of at most about 0.02 and 0.005 Å for parallel and perpendicular positions, respectively, for all listed atoms. This is particularly significant for the deeper atoms near the C_{60}-Cu interface, considering that these atoms are about 7 Å below the outermost C atoms, i.e. about as deep as the electronic mean-free path: this test thus gives confidence in the determination of the interface structure despite its being buried under 7 Å of material.

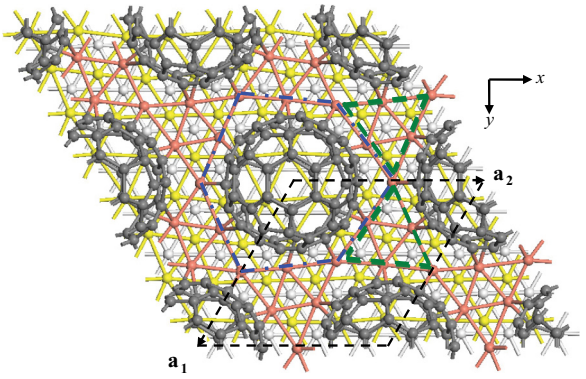

FIG. 4. (Color online) Top view of Cu(111) + (4 × 4)-C_{60} according to our best-fit LEED analysis. Here, $\mathbf{a}_1$, $\mathbf{a}_2$ are basis vectors for the (4 × 4) unit cell (outlined with a dashed black line). Dark gray balls are C atoms; red (gray), yellow (medium gray), and light gray balls are Cu atoms in the first, second, and third Cu layers, respectively. In our right-handed coordinate system, the z axis is perpendicular to the surface and points into the sample; the origin of the x and y coordinates is located at the center of the picture, and the origin of z coordinate is located at the top of a C_{60} molecule.

From our optimized atomic positions, we observe that, for the 101 adjusted atoms, almost all differences in z coordinates between LEED and DFT are smaller than 0.1 Å; the exceptions are three C atoms (group 18, atoms #52, #53, #54 in supplementary material II[18]) which have a difference of about 0.14 Å. There are 32 differences in x and y coordinates larger than 0.1 Å, of which only five differences are larger than 0.2 Å, the largest difference being 0.29 Å (namely for Cu atom #84, located in the second Cu layer, at a depth of about 8.8 Å below the top of the C_{60} molecule). This is consistent with the familiar fact that the LEED analysis is less accurate for the coordinates parallel to the surface and for the deeper atoms due to the mean-free path.

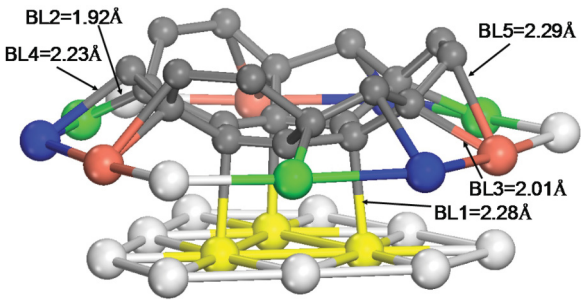

FIG. 5. (Color online) Near-grazing close-up view of the LEED-optimized interface between a C_{60} molecule (small dark gray balls showing only the lower 21 atoms of the buckyball) and r-fcc reconstructed Cu(111) (large balls), showing selected C-Cu bond lengths. Red (gray), blue (medium gray), green (lighter medium gray), and light gray colors denote groups of threefold symmetrically equivalent Cu atoms surrounding the seven-Cu-atom vacancy site (within which the lower C_6 ring is almost coplanar with the remaining Cu atoms). The three outermost light gray Cu atoms are bonded to neighboring C_{60} molecules; the three yellow Cu atoms belong to the second metal layer, together with their surrounding light gray Cu atoms.

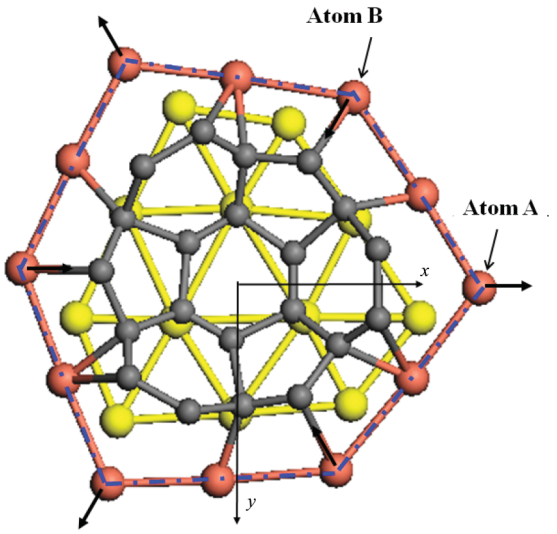

FIG. 6. (Color online) Detailed top view of the LEED-optimized molecule-metal interface: small gray balls are 21 C atoms forming the bottom of the C_{60} molecule; large red balls are Cu atoms of the first Cu layer, forming a distorted hexagon marked by the blue dash-dotted line; large yellow balls are Cu atoms of the second Cu layer.

The seven-atom hole in the outermost Cu layer is clearly visible in Fig. 5 surrounded by a ringlike edge of 12 Cu atoms (colored red, blue, green, and light-gray): the hole is filled with a C_{60} molecule, whose bottom C_6 ring is almost coplanar with the remaining Cu atoms. The edge of the hole is also highlighted in Fig. 4 as a blue dash-dotted line and further magnified in Fig. 6: we observe that this Cu edge is strongly distorted from its original bulklike hexagonal shape (as a result in Fig. 4, the adjacent triangles marked by darker green dashed lines are seen to be significantly rotated in alternate directions).

The cause for the in-plane distortion of the Cu hole edge can be traced to a distinct asymmetrical lateral motion of the bridging Cu atoms (identified by arrows in Fig. 6 and represented by atoms #61 and #63, respectively, in supplementary material II[18]): these Cu atoms, although located midway between two neighboring C_{60} molecules before relaxation from bulklike positions, move sideways by ∼0.30 Å (0.34 Å from DFT). Our LEED error bar [±0.022 Å from Eq. (1) or ±0.12 Å from Eq. (4)] is small enough to view this lateral displacement as distinctly significant, as also confirmed by DFT, showing that these Cu atoms make a stronger bond to one molecule than the other. As seen in Fig. 6, one such atom (at top right) makes a bond to the tip of a C_5 pentagon of the shown C_{60} molecule; other such atoms (e.g. at top left) do likewise, but bond to a neighboring molecule (cf. Fig. 4).

Some edge atoms of the hole (first Cu layer) are also pulled outward (perpendicular to the surface) by the molecule and therefore exhibit a buckling of about 0.07 Å (0.04 Å from DFT) among themselves. Note in Fig. 5 how three Cu atoms in the second Cu layer (yellow atoms) are bonded to the C_{60} molecule: these three Cu atoms are pulled toward the molecule, causing a buckling of ∼0.14 Å (0.08 Å from DFT) in that second Cu layer.

The interface structure between molecule and metal is of particular interest. In Fig. 5, we show all the symmetrically inequivalent distances between C and Cu atoms which are

TABLE II. Cu-C bond lengths (defined in Fig. 5) from DFT (Ref. 8) and LEED (*BL2 and BL3 from DFT were averaged together).

Bond	Length (Å) from DFT	Length (Å) from LEED	LEED precision (Å) [from Eq. (1) with 68% confidence]	LEED accuracy (Å) [from Eq. (4)]
BL1	2.28	2.28	±0.046	±0.15
BL2	2.09*	1.92	±0.068	±0.25
BL3	2.09*	2.01	±0.070	±0.25
BL4	2.28	2.23	±0.077	±0.24
BL5	2.40	2.29	±0.069	±0.25

shorter than 2.30 Å (the sum of the covalent radii of C and Cu atoms is about 2 Å).

The number of C-Cu bonds in this adsorption structure is remarkably large. A total of 12 Cu atoms bond to a single C_{60} molecule: all Cu atoms of the outermost Cu layer (nine atoms per unit cell) bond to C atoms (see Fig. 4), while three Cu atoms per unit cell, located in the second Cu layer just below the C_{60} molecule, also bond to C atoms (with bond lengths within 2.30 Å). Similarly, 15 of the lowest C atoms of a C_{60} molecule (i.e. a quarter of the C atoms) bond to Cu atoms (with bond lengths within 2.30 Å). This large number of bonds illustrates why the adsorption of C_{60} on the Cu(111) surface with seven-Cu-atom holes is very strong and stable.

The C-Cu bond lengths and their uncertainties are shown in Table II. The LEED and DFT results agree well within the accuracy of LEED. This is significant in two ways: first, theory and experiment come to the same structural conclusions; second, the LEED error bars, despite representing uncertainties in atomic positions about 7 Å below the surface, are small enough to allow useful conclusions.

Regarding distortion of the C_{60} molecule, its six-C-atom bottom ring exhibits a buckling perpendicular to the surface of only 0.007 Å in the LEED result (vs 0.027 Å in DFT). The two alternating C-C bond lengths in this ring are 1.507 and 1.279 Å (1.445 and 1.423 Å for DFT), respectively, compared to 1.464 and 1.385 Å for the unrelaxed C_{60} molecule; the LEED accuracy of about 0.26 Å [from Eq. (4)] in these bond lengths leaves this difference indecisive, which is not surprising for deep bonds parallel to the surface. From LEED, the rest of the adsorbed molecule is similarly indistinguishable from its free-molecule structure, while its DFT-optimized coordinates remain within about 0.05 Å of the free-molecule structure, with insignificant changes in the outermost half of the molecule.

In addition, as pointed out by Pai *et al.*,[8] the C_{60} center can sit at either an fcc or an hcp site, depending on whether the top layer Cu atoms are stacked as the unfaulted fcc-like Cu(BACBAC...) denoted r-fcc or as the faulted hcp-terminated Cu(BABCABC...) denoted r-hcp: the DFT energies for C_{60} on these two Cu configurations are nearly identical (as mentioned above, which of these two DFT energies is best switches as a function of the number of Cu layers included in the Cu slab of the model, r-fcc being best for thicker slabs). However, our LEED analysis clearly distinguishes the two models, with best fits of $R_p = 0.377$ and 0.455 for r-fcc and r-hcp stacking, respectively. This illustrates the structural sensitivity of LEED I-V analysis for certain models with nearly degenerate energies.

It is particularly interesting to contrast the current results for C_{60} on Cu(111) with similar adsorption structures of C_{60} on other transition metal surfaces. While C_{60} sinks into a seven-atom hole on Cu(111) and apparently also on Ni(111),[19] C_{60} sits over a one-atom hole on Ag(111)[2] and on Pt(111):[4,5] the local structure of this one-atom hole is very similar to that shown in Fig. 2(c). However, the seven-atom hole structure seen on Cu(111) is also predicted on Ru(0001).[20,21] These different behaviors on different close-packed metals can be traced[21] to a surprisingly simple dependency on substrate lattice constants (and lack of dependency on substrate electronic structures). The near-constant molecule-molecule spacing of C_{60} in its hexagonal monolayer imposes different supercells relative to the different metal substrates, due to their different lattice constants; these different supercells therefore offer different numbers of metal atoms to interact with each C_{60}; for instance, each C_{60} can interact with as many as 16 Cu atoms vs as few as 12 Ag atoms (before reconstruction) in the respective (4×4) vs $(2\sqrt{3} \times 2\sqrt{3})$R30° supercells. The seven-atom hole, which maximizes the number of C-metal bonds, is too large for the smaller supercells: with smaller supercells, metal atoms must share C-metal bonds with two neighboring C_{60} molecules, weakening those bonds: the one-atom hole then becomes more favorable.[21] In both the seven-atom hole and the one-atom hole structures, C_{60} bonds with a hexagon down, which is determined by the symmetry matching between C_{60} and the substrate.[1] The C_{60} mirror planes are perpendicular to those of the substrate in the seven-atom hole structure, while they are parallel to those of the substrate in the one-atom hole structure: these different molecular orientations maximize the number of C-metal bonds of C_{60} to the metal substrate in the different hole structures. C_{60} sinks into the seven-atom hole, bonding with both the atoms at the hole edges and atoms in the second metal layer: this bonding significantly distorts the seven-atom hole structure relative to bulk atomic positions, as shown in Fig. 4; this is different from the one-atom hole reconstructions on Ag(111) and Pt(111), in which only very small displacements of the metal atoms from their bulk positions are detected. These details in the nanopatterning at the molecule-metal interface are essential to the stability of ordered structures of molecules and can critically influence the charge transfer and the C_{60} band structures, which are important aspects in the design of molecular electronic devices.

VI. CONCLUSIONS

Thanks to a considerably larger energy range compared to our earlier study,[8] our new LEED analysis has significantly increased the sensitivity to and reliability of the structure of the interface between C_{60} molecules and a Cu(111) surface. We have shown conclusively that the seven-Cu-atom

vacancy model with Cu fcc stacking is much favored over the one-Cu-atom vacancy model and various nonreconstructed models as well as over a seven-Cu-atom vacancy model with Cu hcp stacking.

Our LEED results, which agree substantially with DFT results, show the intimate bonding behavior between C_{60} and the Cu(111) substrate in the seven-Cu-atom vacancy model that provides a hole or nest for the C_{60} to fit into: in particular, we find that the distances from all Cu atoms of the outermost Cu layer to their closest C atoms in the bottom of the C_{60} molecule are shorter than 2.30 Å, which is true also for three atoms of the second Cu layer. These close distances, coupled with appreciable distortions in the substrate, illustrate the strength of the molecule-metal bonding, consistent with the DFT results.

The seven-atom hole reconstruction found for C_{60} on Cu(111) [and likely on Ni(111)] contrasts with the one-atom hole found on Ag(111) and Pt(111), but coincides with the prediction of a seven-atom hole on Ru(0001). These different behaviors have been traced to a simple dependency on metallic lattice constants.[21]

ACKNOWLEDGMENTS

This work was supported in part by CityU Grant No. 9610059 and by the CityU Centre for Applied Computing and Interactive Media. W.W.P. and H.T.J were supported by NSC, NCHC, and NCTS, NTU, Taiwan.

---

*Current address: Institute of Computational and Theoretical Studies, Hong Kong Baptist University, Kowloon, Hong Kong, China.
†Corresponding authors: wpai@ntu.edu.tw, vanhove@hkbu.edu.hk

[1] X. Q. Shi, M. A. Van Hove, and R. Q. Zhang, J. Mat. Sci., doi: 10.1007/s10853-012-6361-y (2012).
[2] H. I. Li, K. Pussi, K. J. Hanna, L. L. Wang, D. D. Johnson, H. P. Cheng, H. Shin, S. Curtarolo, W. Moritz, J. A. Smerdon, R. McGrath, and R. D. Diehl, Phys. Rev. Lett. **103**, 056101 (2009).
[3] M. Stengel, A. DeVita, and A. Baldereschi, Phys. Rev. Lett. **91**, 166101 (2003).
[4] R. Felici, M. Pedio, F. Borgatti, S. Iannotta, M. Capozi, G. Ciullo, and A. Stierle, Nat. Mater. **4**, 688 (2005).
[5] X. Q. Shi, A. B. Pang, K. L. Man, R. Q. Zhang, C. Minot, M. S. Altman, and M. A. Van Hove, Phys. Rev. B **84**, 235406 (2011).
[6] W. W. Pai, C. L. Hsu, M. C. Lin, K. C. Lin, and T. B. Tang, Phys. Rev. B **69**, 125405 (2004).
[7] W. W. Pai, C. L. Hsu, K. C. Lin, and T. B. Tang, Appl. Surf. Sci. **241**, 194 (2005).
[8] W. W. Pai, H. T. Jeng, C. M. Cheng, C. H. Lin, X. Xiao, A. Zhao, X. Zhang, G. Xu, X. Q. Shi, M. A. Van Hove, C. S. Hsue, and K. D. Tsuei, Phys. Rev. Lett. **104**, 036103 (2010).
[9] See Supplemental Material I at http://link.aps.org/supplemental/10.1103/PhysRevB.86.075419 for LEED experimental IV-data of Cu(111) + (4 × 4)-C_{60}.
[10] L. L. Wang and H. P. Cheng, Phys. Rev. B **69**, 045404 (2004).
[11] P. J. Rous and J. B. Pendry, Surf. Sci. **219**, 355 (1989).
[12] M. A. Van Hove, W. Moritz, H. Over, P. J. Rous, A. Wander, A. Barbieri, N. Materer, U. Starke, and G. A. Somorjai, Surf. Sci. Rep. **19**, 191 (1993).
[13] A. Barbieri and M. A. Van Hove: software available at http://www.icts.hkbu.edu.hk/vanhove/.
[14] M. A. Van Hove, W. H. Weinberg, and C.-M. Chan: *Low-Energy Electron Diffraction* (Springer-Verlag, Berlin Heidelberg New York London Tokyo, 1986), p. 251–253.
[15] H. D. Shih, F. Jona, D. W. Jepsen, and P. M. Marcus, Surf. Sci. **104**, 39 (1981).
[16] R. E. Walpole and R. H. Myers, *Probability and Statistics for Engineers and Scientists* (MacMillan, New York, 1972).
[17] J. B. Pendry, J. Phys. C **13**, 937 (1980).
[18] See Supplemental Material II at http://link.aps.org/supplemental/10.1103/PhysRevB.86.075419 for the atomic coordinates obtained by LEED and DFT.
[19] C. H. Lin, K. C. Lin, T. B. Tang, and W. W. Pai, J. Nanoscience Nanotech. **8**, 602 (2008).
[20] J. Lu, P. S. E. Yeo, C. K. Gan, P. Wu, and K. P. Loh, Nature Nanotech. **6**, 247 (2011).
[21] X. Q. Shi, M. A. Van Hove, and R. Q. Zhang, Phys. Rev. B **85**, 075421 (2012).